UNIVERSITY OF CALIFORNIA,
IRVINE

Analysis of Corneal Change Mechanisms Through Second Harmonic Generation Microscopy

THESIS

submitted in partial satisfaction of the requirements
for the degree of

MASTER OF SCIENCE

in Biomedical Engineering

by

Pamela Ann Borden

Thesis Committee:
Dr. Brian J Wong, Chair
Professor Elliot Botvinick
Professor Jared Haun

2020

DEDICATION

To

my caring family, particularly my parents and sister,

and my friends, co-workers, and colleagues,

who have helped and supported me throughout the trials and tribulations

that come with graduate school.

TABLE OF CONTENTS

LIST OF FIGURES

Page

LIST OF TABLES

Page

ACKNOWLEDGEMENTS

I would like to express the deepest appreciation to my faculty advisor, Dr. Brian Wong, who supported me throughout my graduate and undergraduate experience. He helped me learn how to present, analyze, and question research, even when projects slowed due to unprecedented times. Without his understanding and support of me being a full-time student and part-time worker, this thesis would not be possible.

I would like to thank all of my lab mates who have provided guidance and help throughout this research. Seeing the ambition everyone has, particularly the undergraduates and volunteer high school students, is inspiring and constantly reminded me to push myself. This was especially admirable considering the extreme uncertainties presented during the COVID-19 pandemic. They are all extraordinary individuals who deserve nothing but the best.

To all my friends I have met during this program who have only been supportive and kind during this unpredictable graduate career, I can only express my greatest gratitude. I am thankful to have gotten to know all of them and their diverse backgrounds before online learning was implemented.

Lastly, to my family who has constantly supported me during all the good and bad moments that come with graduate school. They always remind me if thousands of people have completed graduate programs, I can do it too.

ABSTRACT OF THE THESIS

Analysis of Corneal Change Mechanisms Through Second Harmonic Generation Microscopy

by

Pamela Ann Borden

Master of Science in Biomedical Engineering

University of California, Irvine, 2020

Dr. Brian J. Wong, Chair

Second harmonic generation (SHG) microscopy has been a widely used method to image collagen-based tissues due to its non-invasive nature and ability to determine collagen changes with appropriate analysis. This technique has recently been applied to analyze the collagen structure of fresh corneal tissue, overcoming the limitations and challenges that occur with traditional microscopy and imaging techniques requiring fixation and dyes. Orientation and organization of the corneal collagen fibers is critical for optimal transparency and optical functionality. Corneal chemical injuries (CCIs) may result in the cornea to become opaque and thus obscuring vision. Other conditions, such as myopia or astigmatism, are a consequence of corneal shape deviations. Current treatments for vision correction are invasive, costly, or fail to fully restore a patient's vision. Most corneal reshaping methods are either passive using rigid/semi-rigid contact lenses to gradually alter corneal shape (orthokeratology) or rely upon laser technology to perform precision ablation of corneal tissue. An alternative approach relies upon the in-situ generation of localized pH gradient that alter stress-strain relationships within the cornea, leading to potentially sustained shape change. This novel, minimally invasive approach ("electrochemical

therapy"- ECT) is currently being evaluated to clear corneal opacification following a chemical injury and corneal reshaping. ECT has been previously used to reshape cartilage and chemically alter the collagen structure of skin.

The objective of this thesis is to study corneal collagen structure using SHG microscopy to examine chemical injuries and electrochemical reshaping. Image processing techniques were developed to gauge structural changes observed with SHG imaging. Fresh ex-vivo rabbit corneas were imaged using SHG. Native fresh corneal tissue was examined and compared with alkaline-injured corneas before and after ECT-clearing. ECT reshaped cornea was examined as well. The extracted images were then processed through ImageJ and a customized MATLAB code to determine the collagen fiber orientation and compared to identify potential statistical indicators of structural change. Collagen distribution patterns throughout the thickness of the cornea were determined in all samples. Knowledge of the collagen structure obtained through SHG combined with white light photography and microscopic data provides information of the changing corneal extracellular matrix. This analysis can be utilized for collagen studies for future projects.

Chapter 1: Cornea Injuries and Conditions

1.1 Collagen Structure of Cornea

The cornea is one of the few transparent tissues found in animals [1]. Certain conditions contribute to the cornea's transparency: configuration of the collagen, avascularity of the stroma, and the smooth refractive surface of the surface epithelium and the tear film [2]. The schematic seen in Figure 1 shows how the cornea is composed of 5 layers: the epithelium, Bowman's layer, the stroma, Descemet's membrane, and the endothelium. The corneal structure has previously been studied through the use of histology and traditional microscopy, which requires the tissue to be fixed.

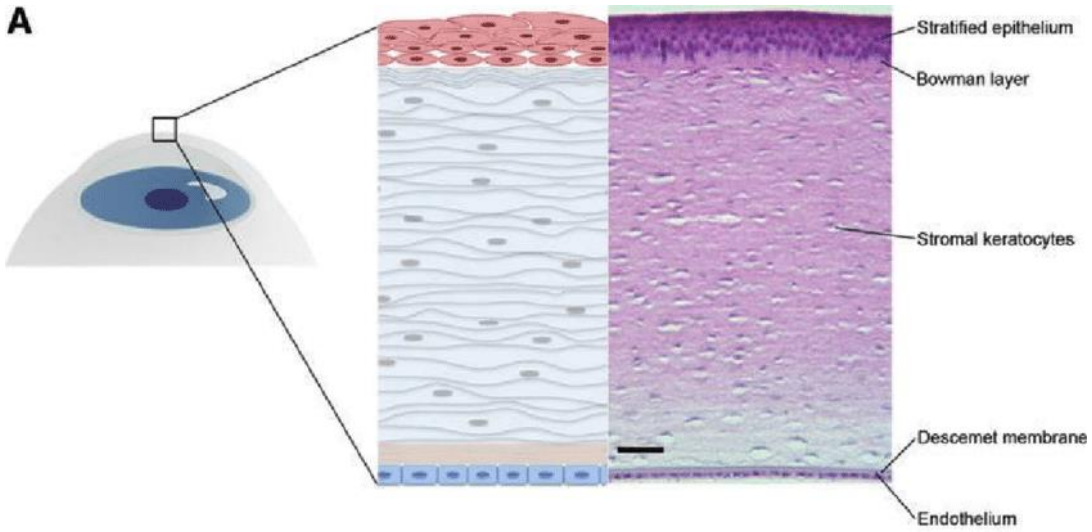

Figure 1: Schematic showing the 5 layers within the cornea [3].

The stroma is the central layer of the cornea and accounts for approximately 90% to the corneal thickness [4]. This ocular component is mostly composed of type I collagen, a fibrillar type which has specific structural composition commonly seen in connective tissues. Configuration of the collagen is critical as these bundles maintain a specific geometric shape and orientation throughout the cornea. This can be seen in the stroma as each fibril with

approximate diameters of 10-20nm are distanced from each other at a fixed length of 20 nm. By keeping these collagen patterns, the cornea remains compliant with the "lattice theory" where the regular arrangement reduces interference of scattered light outside of the incident beam as the fibrils cause destructive interference [5]. By minimizing scattering, the cornea is able to retain full transparency and functionality.

1.2 Opacity of Cornea

Corneal opacity may be triggered for various reasons such as trauma, disease, and infection [6]. Corneal chemical burns (CCIs) contribute to 11-22% of all ocular injuries and may lead to corneal opacity and tissue ischemia [7]. Chemical burns are a result of exposure to either acid or alkaline solutions due to the victim's occupational industry such as agriculture or industry. Acids damage the outer most layers by causing the proteins of the cell to congeal and are less severe due to the coagulation of the tissue preventing further penetration of the agent. Alkali injuries can be more severe since these solutions are lipophilic and easily diffuse deeper as so coagulum forms.

Current treatment is dependent on the classification of the injury using the Roper-Hall classification system which evaluates the eye's corneal haze and ischemia [8]. The lowest classification of I indicates some corneal epithelial damage whereas the highest classification of IV identifies complete opacity of the cornea with some limbal ischemia. Irrigation with an aqueous solution, preferably with a type of saline solution, is always the immediate action in an attempt to flush the irritant out of the eye and to correct the ocular pH [9]. Topical corticosteroids are used for varying durations depending on injury severity to reduce inflammation and cellular release of matrix-degrading enzymes. Although this may help

reduce swelling, further treatment is required to resolve cornea opacity and ischemia. Viability of the limbal stem cells is critical as it prevents the conjunctival tissue from overgrowing into the cornea, which causes stromal neovascularization, which further destroys clarity and leads to scarring [9]. Corneal transplantation may be an option to cosmetically resolve the issue, however if the limbal stem cells of the eyes are severely damaged, then full-functionality restoration is unachievable. Depending on the surgery performed, the patient may require immunosuppressants in order to prevent the risk of immunologic graft rejection after transplantation.

Previous studies explored the use of direct corneal surface electrolysis as an alternative potential solution from *lamellar keratoplasty* (LKP) and *penetrating keratoplasty* (PKP) to resolve corneal and subepithelial opacity as patients undergoing these surgeries have experienced recurring corneal clouding [10], [11]. Surface electrolysis clears the cornea through breakdown of the corneal deposits by hydrolyzing water with an applied voltage. This work will focus on the effects a novel corneal clearing technique that capitalizes similar electrolysis concepts may have on the collagen structure of the stroma.

1.3 Irregular Corneal Shaping

Vision is dependent on incoming light accurately hitting the focal point on the retina. Refractive errors occur when the light taken in by the eye is unable to correctly reach this area. Myopia, which focuses light in front of the retina, presbyopia, where the lens is unable to adjust for close objects, and astigmatism are direct results of refractive errors. The American Academy of Ophthalmology has found that 8.4% of Americans have hyperopia, 23.9% have myopia, and 33% have astigmatism [12]. Many of these conditions are linked

with a suboptimal contour of the corneal surface due to genetics as well as environmental components.

Current therapies to correct these errors include spectacles, contact lenses, photorefractive surgery (e.g. Lasix), and even pharmaceuticals [13]. Spectacles are an easy solution as the lenses are customized to the patient's needs; however, patients will need to change their prescriptions over time or may require a transition to bifocal lenses if treating for presbyopia. Contact lenses may be used to compensate for an irregular corneal surface, but they require continuous care and cleaning to prevent eye infections. For astigmatism, specialized rigid contact lenses are worn to reshape the cornea during limited time periods and then removed to temporarily restore vision [14]. Laser operations such as *laser in situ keratomileusis* (LASIK) and *photorefractive keratectomy* (PRK) are commonly used to reshape an eye experiencing refractive errors due to an irregular corneal surface [15]. Figure 2 shows the procedure for LASIK surgery to remove tissue and reshape the cornea using a femtosecond laser. Lastly, pharmaceuticals have been developed in attempts to reduce these errors through crystalline lens softening or expansion of depth of focus [16]. These therapies face various issues concerning longevity, expense, and invasiveness.

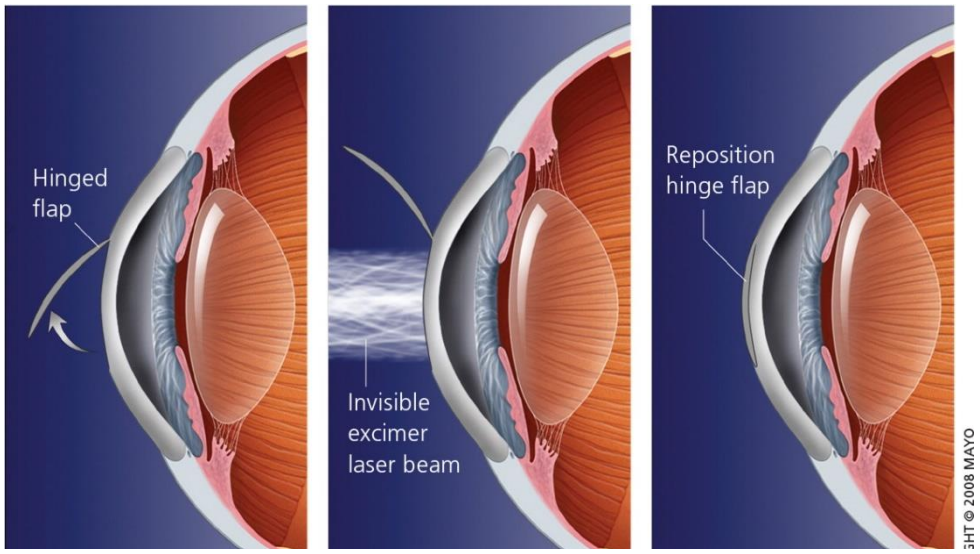

***Figure 2**:* Schematic demonstrating the procedure for performing LASIK surgery [17].

Electromechanical reshaping (EMR) treatments have been used in other tissue applications such as tendon elongation, cartilage reshaping, visible scar reduction, and fat reduction [18], [19], [20], [21]. Through EMR, the sample is directly exposed to a conductive contact which will apply a current and a mechanical force on the region of interest. The in-situ redox reactions occurring within the specimen's structural matrix will then allow the tissue to deform. Severity of deformation is dependent on the length of time the contact is applied and the voltage strength [22]. This work will focus on the effects a novel corneal EMR technique may have on the collagen structure of the stroma.

Chapter 2: Second Harmonic Generation Microscopy

2.1 Background and Applications

Previous biomedical imaging techniques focused on linear methods that relied on observation of linear interactions with the specimen such as light absorption, refraction, scattering and fluorescence. These microscopy methods provide three-dimensional resolution of the specimen but are limited by shallow imaging depth into the tissue and potentially phototoxicity (in the UV light spectra). Because phototoxicity can damage the specimen, tissues examined using classic light microscopy must be fixed prior to imaging, preventing real-time study of cellular interactions.

Within the past decade, advancements in nonlinear optical microscopy techniques, such as second harmonic generation (SHG), have been developed to overcome these limitations. Nonlinear optical microscopy works by having the polarization density ($\boldsymbol{P}$) of the imaged material give a nonlinear response to the incoming light's electric field strength ($\boldsymbol{E}$) (2-1) [23].

$$\boldsymbol{P}(t) = \epsilon_0[\chi^{(1)}\boldsymbol{E}(\mathrm{t}) + \chi^{(2)}\boldsymbol{E^2}(\mathrm{t}) + \chi^{(3)}\boldsymbol{E^3}(\mathrm{t}) + \cdots] \qquad (2\text{-}1)$$

Where ϵ_0 is the permittivity of free space and $\chi^{(n)}$ are the first-order, second order, and third-order susceptibility. By using nonlinear microscopy, researchers are able to image to a greater depth in tissue with high sensitivity and resolution. This facilitates observation the structural changes with depth and limited phototoxicity. As a result, living tissues can be examined using nonlinear techniques to allow for analysis on tissue function over time. Endogenous molecular markers can also be investigated through this process, providing the

opportunity to understand how cellular structures display relationships between organ and tissue function.

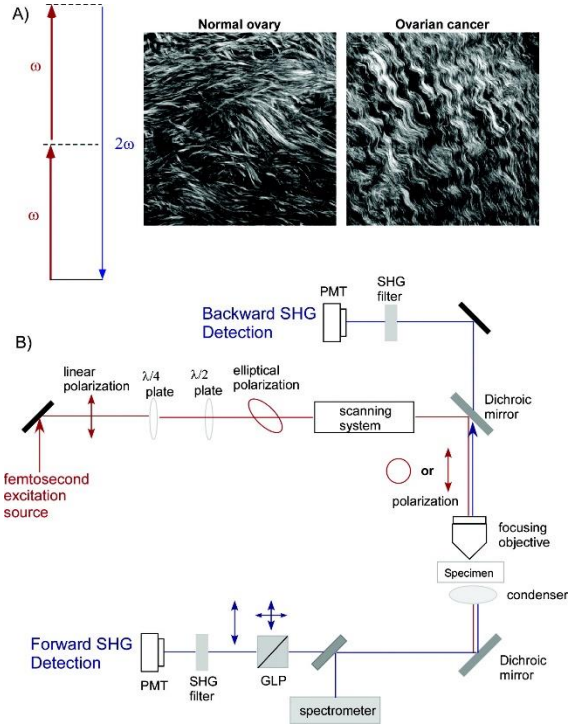

***Figure 3**:* Representation of how images are captured through SHG microscopy through the energy created from two photons (A) and the appropriate mirrors and filters [24].

SHG imaging is a process involving second-order nonlinear optical susceptibility, $\chi^{(2)}$. Two lower energy photons at an incident frequency (ω) generate a single photon that has twice the frequency (2ω) of the excitation femtosecond or picosecond laser, which is depicted in Figure 3A [25]. This phenomenon occurs when the excitation laser passes through highly ordered and non-centrosymmetric materials, making it ideal to analyze biological tissues such as collagen, muscle, and extracellular matrix (ECM) components [23]. Multiphoton imaging allows for visibility at the molecular level of structures or even metabolic activity, focusing beyond the cellular structures.

SHG has been previously used to image and analyze collagen structures of various tissues due to the technique's high sensitivity to these ECM components and potential changes. The classification of collagen type within a sample tissue is critical to understand as this will determine the SHG signal strength. Type I collagen is the most abundant type found in the body and gives one of the strongest SHG signal due to its heterotrimeric and non-centrosymmetric structure [26]. This has enabled research into collagen fibril structures for connective tissues, internal organs, blood vessels, and cornea.

Collagen arrangement of the human cornea can now be investigated using SHG, though there are limited reports to date. Studies have shown that the collagen bundles maintain unique arrangements at various depths and locations within the cornea [27]. Analysis of the corneal structure allows for deeper understanding on how they contribute to optical function. Additional studies have used SHG to quantitatively compare healthy cornea structures to diseases ones diagnosed [25]. In diseased corneas with keratoconus, where the cornea thins and starts to bulge outward, or pseudophakic bullous keratopathy, where there's stromal edema, it has been shown that their collagen fibers do not maintain regular distributions with a clear preferred orientation.

2.2 Image Processing and Data Analysis

In this study, ImageJ, an open source imaging software, and a customized MATLAB code are the primary tools used to post-process image data. SHG images were acquired with a Zeiss LSM 510 Meta inverted confocal microscope where an excitation wavelength of 920 nm was used. SHG z-stacks sizing 900um by 900um captured depths that were on average approximately 150um with varying steps depending on the experimental setup. Additional

cross-sectional tile images (9000um by 9000um) were acquired to evaluate the overall spatial distribution and orientation of corneal collagen. Z-stack images were processed through ImageJ using the OrientationJ plugin that was developed by the Biomedical Imaging Group in Switzerland [28]. This plugin provides a function called *Distribution* which characterizes the orientation and isotropy properties of the collagen in the image by evaluating the gradient structure tensor of the local neighborhood of the selected image. The tensors were evaluated using a Fourier gradient within a local window size of 1 pixel. The resulting instances of found orientation angles are displayed and set on a range from -89.5^{o} to +89.5^{o}. To accommodate for the potential changes in the cornea placement during the before and after imaging sessions, additional analysis isolating a region of interest (ROI) was performed. Figure 4 illustrates how the cross-sectional tile images taken at before and after were concentrically stacked through ImageJ to identify a reference area to directly compare the accompanying z-stacks of the control and treated corneal centers. The ROIs were processed through OrientationJ's function, *Measure*, which calculates the directional coherency coefficient of the collagen fibers at each step in the taken z-stacks.

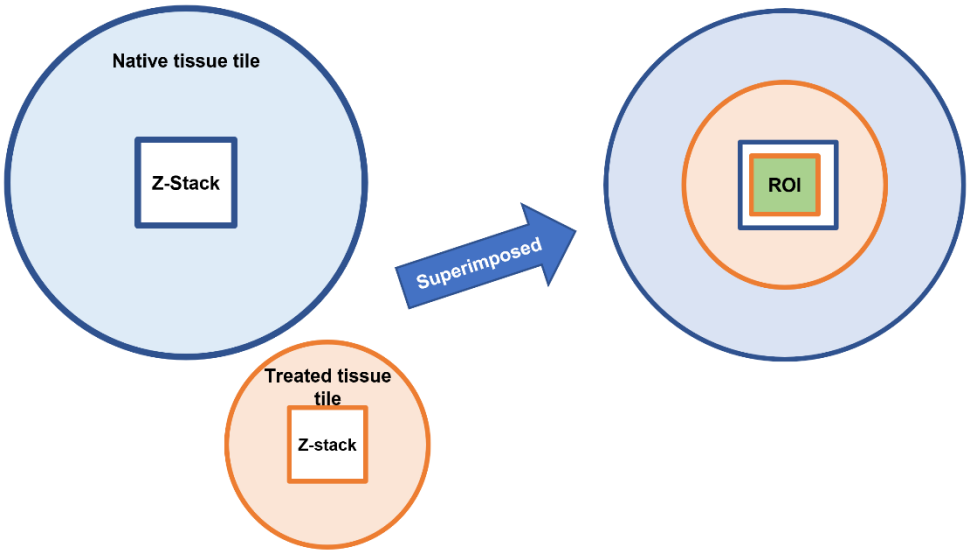

Figure 4: Native and treated tile images captured are superimposed through ImageJ to determine the ROI, represented in green, for coherency analysis.

A customized MATLAB code was developed to extract the orientation data from OrientationJ's *Directionality* function to analyze the preferred collagen fiber orientation and standard deviation both before and after data filtering. The data was filtered out the lowest observed frequencies to remove noise and the angles were rounded to the nearest degree to analyze the set from -90^{o} to $+90^{o}$. The number of occurrences of a tensor calculated at a specific angle were converted into normalized decimal numbers ranging from 0 to 1 in order to facilitate direct comparison between all datasets. Because the ImageJ plugin function gave orientation in 0.5-degree increments without a zero, an artificial zero degree point was generated to center the data by computing the average occurrence between -0.5 degrees and 0.5 degrees as these were the angles closest to zero. Once data was filtered and normalized, the preferred orientation angle was determined by taking the mean of the data at each image in the z-stack. Standard deviation was also calculated at every z-stack slice to show if the preferred orientation, or mean orientation, is uniform across all collagen fibers within that image.

Chapter 3: Analysis of Mechanisms for Corneal Manipulation

3.1 Corneal Clearing

3.1.1 Experimental Setup

For corneal clearing experiments, White New Zealand rabbit eyes were extracted within three hours post-mortem. Globes were extracted and placed in room temperature sterile saline. To ensure tissue was fresh, imaging and experiments began within two hours. Previous damage to the corneal surface was evaluated prior to any treatments through SHG imaging. Scratches or major defects due to external factors, such as the rabbit scratching its eye prior to euthanasia or damage during post-mortem enucleation preclude use of the specimen for experimental protocols and thus are used as controls for native corneal structure. Intact globes were removed from the saline and placed with the cornea facing downward toward the objective lens. The surface of the cornea was maintained in direct contact with a transparent cell culture dish which provides a base of support during SHG imaging. An annular shaped saline-soaked sponge was placed along the edge of the dish, stabilizing the sample during imaging to prevent it from moving and changing orientation. Additionally, the sponge supported the globe, reducing the deformation produced by the weight of the eye against the culture dish. This reduced the potential for creating artifacts such as corneal wrinkles. By saturating the cushioning in saline, the cornea remained moist during imaging.

The entire assembly was secured and positioned on the viewing platform of the inverted confocal microscope. An excitation wavelength of 920nm was used during the two-photon microscopy to view the collagen structure. First, a cross-sectional 9000umm-by-

9000um tile image was taken to capture the entire corneal surface at approximately 150um depth to provide a broad landscape image of the organ. Second, 900um-by-900um z-stacks with a minimum thickness of 150 um and a 10um step between slices, were acquired at the center of the cornea as determined by the tiled image data set. Once initial baseline images were captured, the globes were placed back into the saline solution to be prepared for additional optical coherence tomography (OCT) imaging and then experimental treatment.

Globes were transferred with the cornea facing upwards to a customized silicone jig with a concave cavity to stabilize the specimen. Saline-soaked blotter paper was placed within the cavity beneath the eye to help preserve moisture and prevent excessive movement. This jig was then held in a 100-mm wide crystallizing dish and put on a Z-adjustable stage to allow image focusing for the OCT system. Digital photographs or video were recorded during all stages of treatment for supporting qualitative data.

Three platinum electrodes were used to perform electrochemical therapy (ECT) on specimens for the experimental group. The anode, or the working electrode, was laid flat across the center of the cornea. The cathode, or the counter electrode, was inserted between the eye and the edge of the jig's cavity. Lastly, the reference electrode was placed in contact with the cornea near the working electrode to close proximity of the working electrode to measure the potential of the anode. Figure 5 shows the full experimental setup of the electrodes in relation to the sample eye. The CH Instruments 650A potentiostat/galvanostat ECT system was used with its settings controlled through the complimentary software, CHI650A Electrochemical Workstation. The bulk electrolysis technique was selected with the electrolysis potential parameter set to 1.5V and a preelectrolysis potential of 0V. By using

this method, a specified, constant potential is applied to the corneal surface for a certain time. For this application, it allows for the creation of a localized in situ pH gradient from the working electrode.

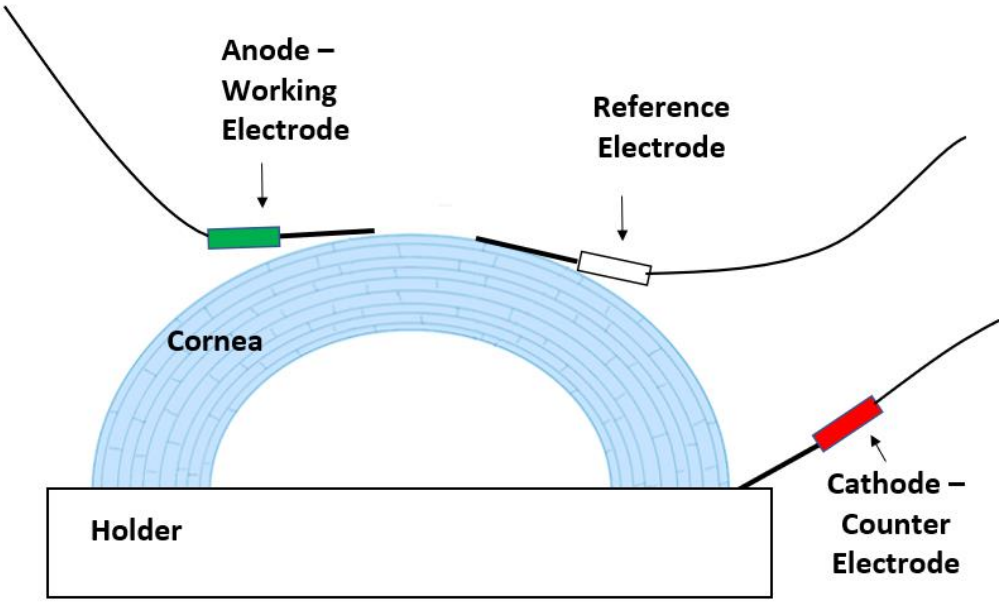

***Figure 5**:* Electrode configuration during electrochemical therapy used for corneal clearing

To simulate alkali damage, the cornea had 1.5 mL of NaOH pipetted directly onto its surface with exposure lasting for approximately 60 seconds. The damaged cornea was flushed with room temperature tap water using a pipette for ten minutes to replicate similar recommended initial clinical treatment for a base injury in an attempt to normalize the eye's pH gradient [29]. A set of samples was set aside after NaOH treated to serve as the negative control group for later comparison.

After NaOH exposure, experimental group samples had bulk electrolysis applied to them at 1.5V for approximately fifteen minutes. OCT imaging was performed throughout the entirety of all protocols for supplemental data. SHG was performed once more following the same initial procedure after each completed treatment to determine any changes in the

presence and structure of collagen. Collagen alignment data analysis was performed on the SHG images through ImageJ's plug-in, OrientationJ, and a customized MATLAB script.

3.1.2 ***Results***

Prior to analysis of the SHG images, a survey of the optical images was done to review the qualitative baseline and treated states of the negative control and experimental samples. Images of the native cornea show optical clarity with full view of the iris and pupil and no obvious surface defects or deformities. After application of the NaOH solution, opacification occurs instantaneously and is classified as a grade IV injury on the Roper-Hall Classification scale where the cornea is opaque, and the iris and pupil are obscured. This class of injury would typically require surgery such as an amniotic membrane transplant because of severe damage to the ocular surface [30]. After ECT treatment, partial optical clarity appears to be restored in the contact area underneath the anode electrode. Figure 6 is a montage that compares the samples both before and after treatments.

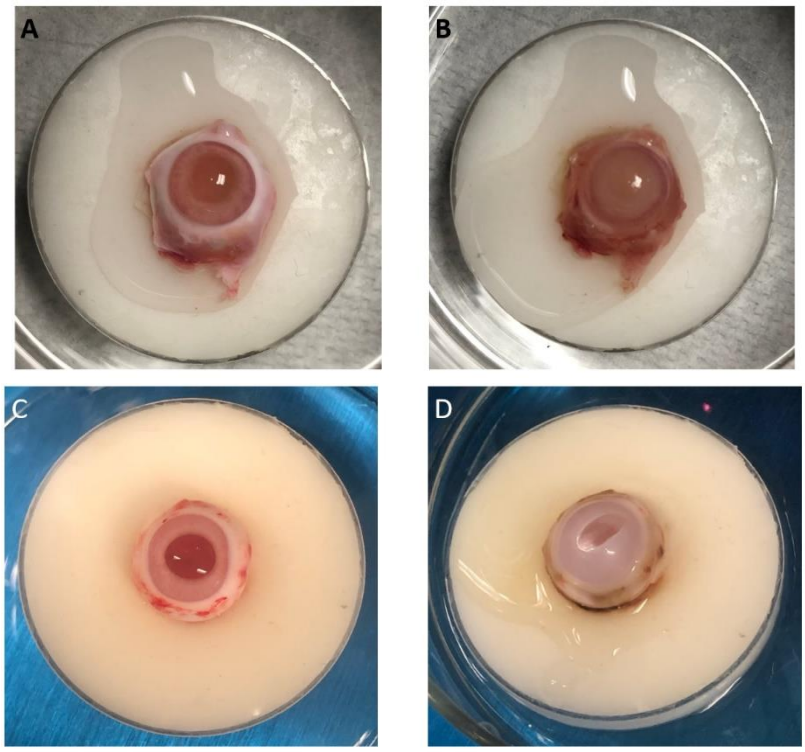

Figure 6: Optical images showing corneal opacity for alkaline-treated cornea (**A** and **B)** and NaOH+ECT treated cornea (**C** and **D**).

Native corneal tissue prior to any treatment exhibits a blue, fluorescent signal through SHG, representing the abundance of collagen fibers. Figure 7 shows the tiled images of the control over the entire corneal surface. Some of the images have minor dark areas due to physical damage from mechanical trauma that occurred during globe extraction or scratches acquired prior to euthanasia, as globes were freshly obtained from subjects euthanized for other IACUC approved protocols. After alkaline exposure, the corneal tissue had significantly reduced collagen signal intensity. Absence of the fluorescence indicates that structure of the collagen fibers has been disrupted or damaged. ECT treatment after NaOH exposure appears to provide a stronger collagen signal in and around the region affected by bulk electrolysis. The tissue outside of the ROI, which is still opaque from the alkaline damage, displays little to no collagen signal.

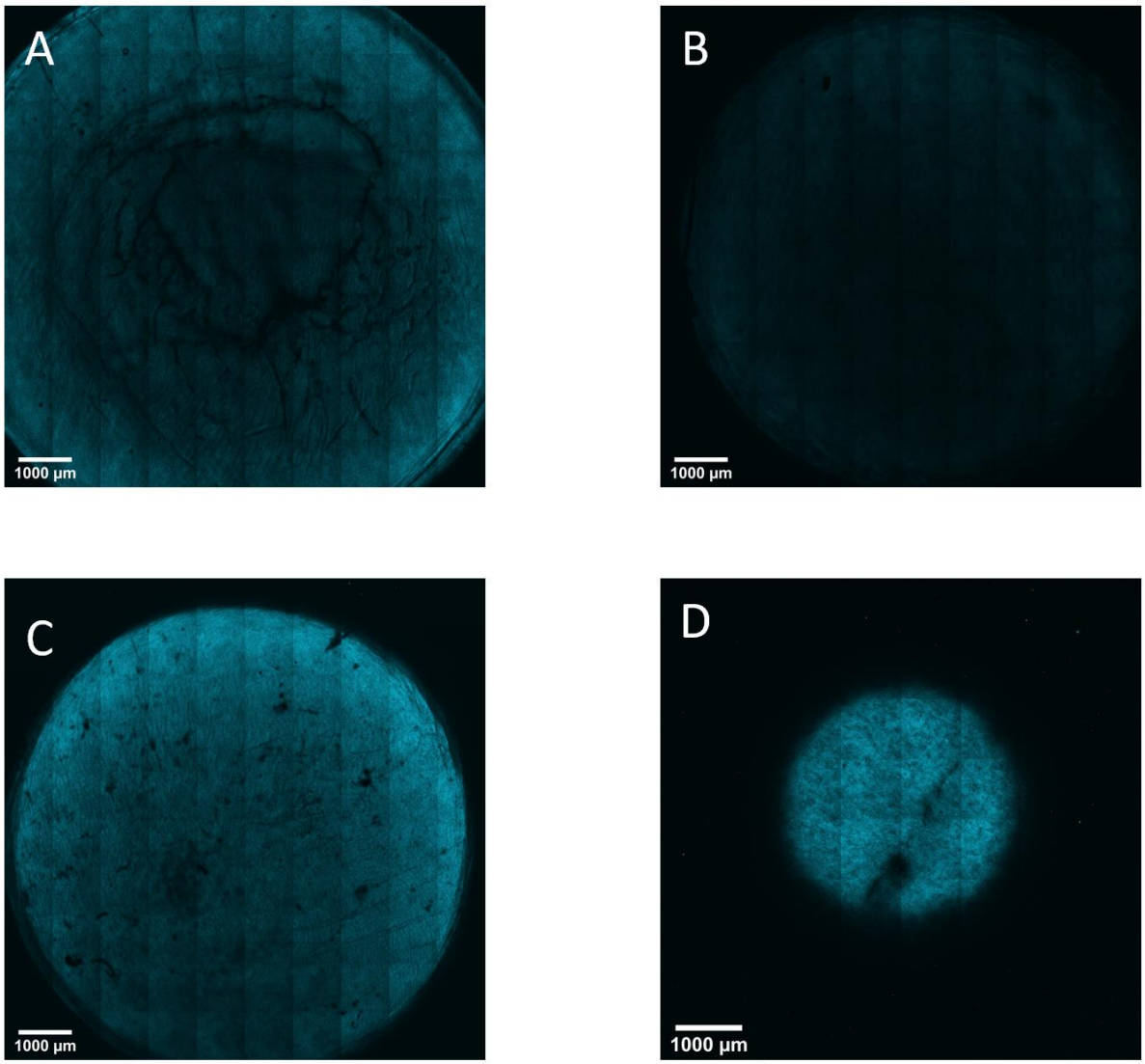

Figure 7: SHG images acquired of the corneal opacity for alkaline-treated cornea (A and B) and NaOH+ECT treated cornea (C and D). Blue signaling represents the presence of collagen.

Z-stacks were generated at the center of the cornea for all datasets and were analyzed to determine the collagen fibril orientations throughout all tissue depths. The histograms in Figure 8 show that the collagen fibers retain a Gaussian distribution of orientation for all protocols at depth of 150-micron within the cornea. In as much as the stroma begins at a depth of approximately 70-microns deep within the cornea, a depth of 150 microns was chosen for further analysis as this ensured image acquisition was definitively in the stroma.

This is where the bulk of corneal collagen is located. Compared to native cornea tissue orientation, the negative control minimally altered the preferred mean collagen orientation angle by approximately 2.13 degrees. The standard deviation shifted as well, increasing the directionality by 1.77 degrees from the control sample. The experimental cornea showed the preferred mean collagen orientation angle decreased by 3.93 degrees and the standard deviation of directionality was nearly identical with a difference of only 0.39 degrees. These results suggest that the cornea's collagen organization and alignment are minimally changed by the introduction of NaOH and the induced pH gradient generated from the ECT treatment. This is summarized in Table 1.

Treatment	Collagen Orientation Mean (Degrees)	Collagen Orientation Standard Deviation (Degrees)	Coherency
Control	-0.85856	32.6435	0.033
NaOH	1.267	34.422	0.033
Control	2.8682	32.3195	0.048
NaOH + ECT	-1.0707	32.7106	0.038

***Table 1**:* Comparison of calculated values from SHG images taken at 150um depth of control and treated corneas analyzed through ImageJ for collagen fibril orientation mean, standard deviation, and coherency.

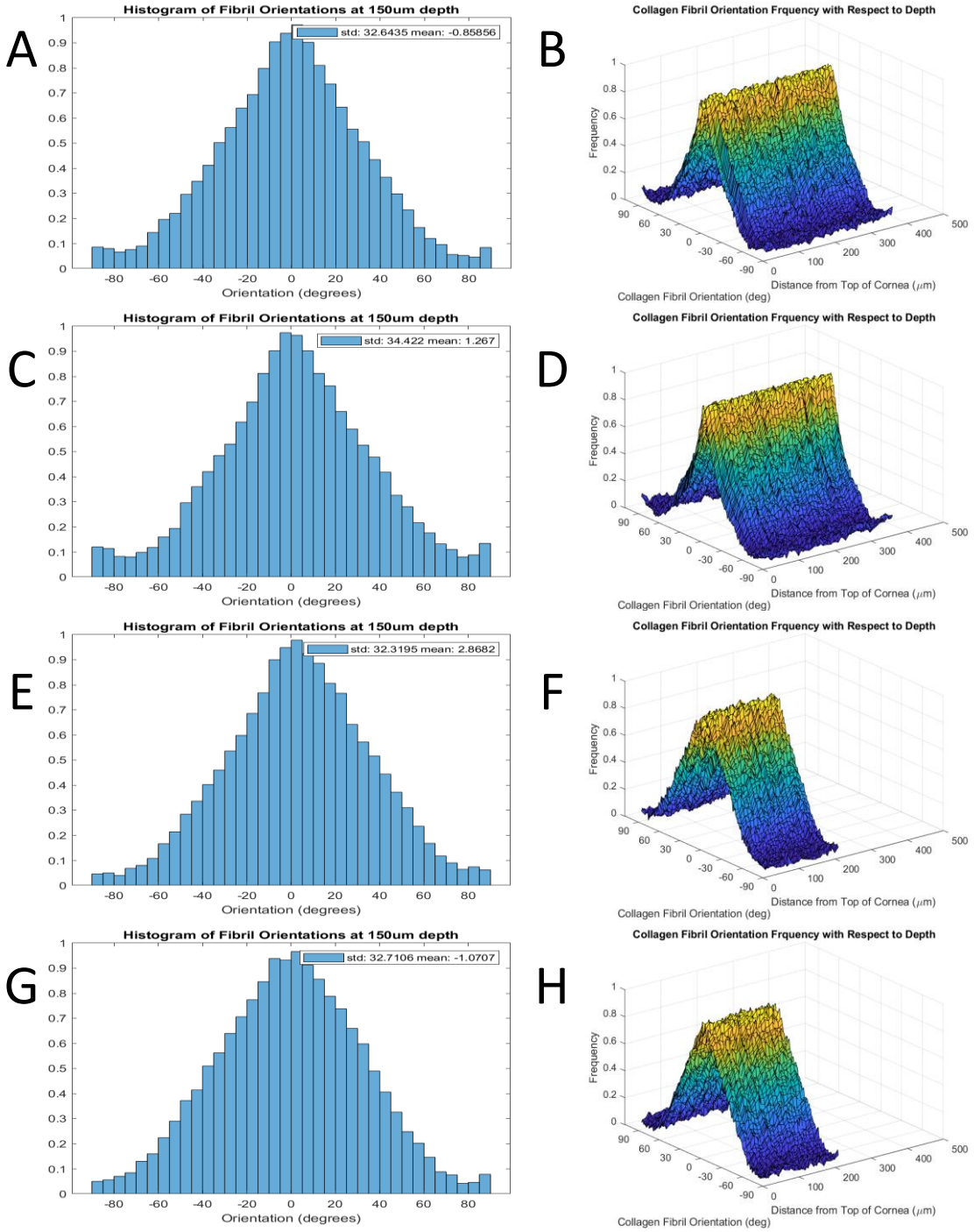

Figure 8: Collagen fibril orientations showing the preferred orientation frequency histogram as well as orientation in relation to depth from SHG z-stack images. Rows 1 and 2 give data for the native (A and B) and alkaline-treated cornea (C and D) respectively. Rows 3 and 4 show data for the native (E and F) and NaOH+ECT treated cornea (G and H) respectively

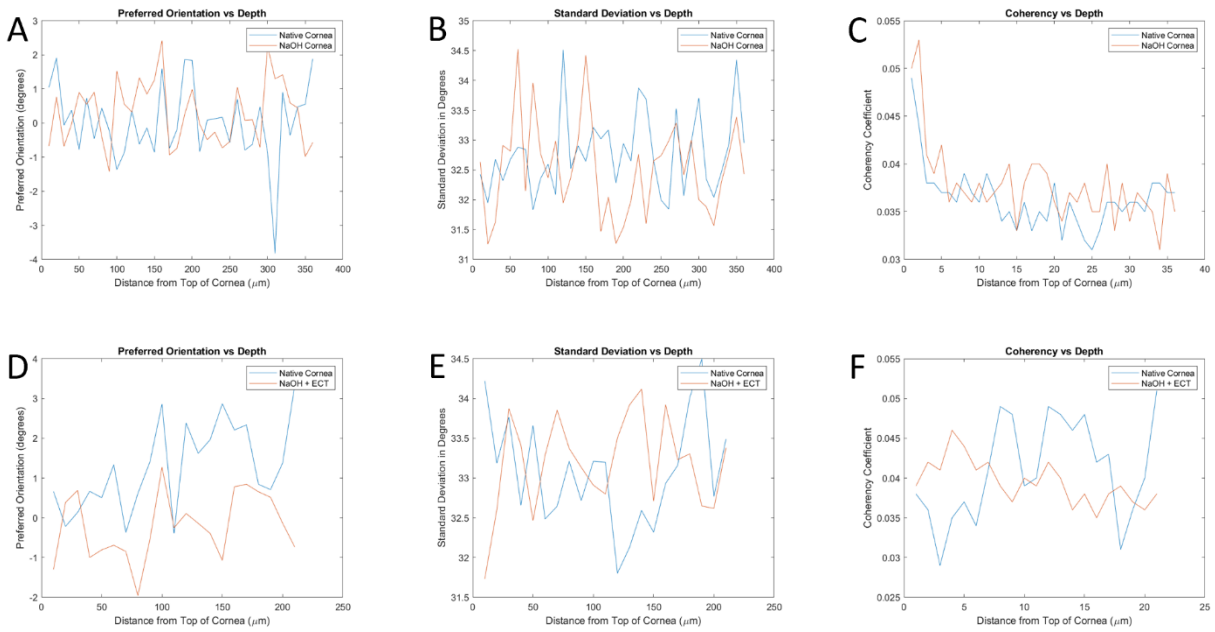

Figure 9: Evaluation of preferred orientation (A), standard deviation (B), and coherency (C) with respect to depth in base-treated corneas compared with its control. Data analysis also performed on NaOH+ECT treated tissues (D, E, F).

To confirm the small change in collagen orientation between the control and treated samples, additional analysis was performed to examine the overlapping ROIs. Figure 10 is an overlay of the tile SHG images of the native and treated corneas. They were digitally aligned in software to improve registry so that the selected ROI from the z-stacks taken at the center were concentric. OrientationJ was used for processing to determine the ROI's coherency coefficient (Table 1) of the different treatments, which indicates if the ROI has a preferred orientation if the coefficient is close to 1 [31]. No change in tissue coherency was observed between the negative control sample (NaOH) and the native cornea specimens. This implies there showing no preferred orientation. Coherency decreased between the NaOH+ECT treated and native cornea by 0.1, but this value still does not show a significant change in preferred orientation of the collagen fibers. Figure 9 displays orientation mean,

standard deviation, and coherency with respect to depth for both the alkaline-treated and cleared samples.

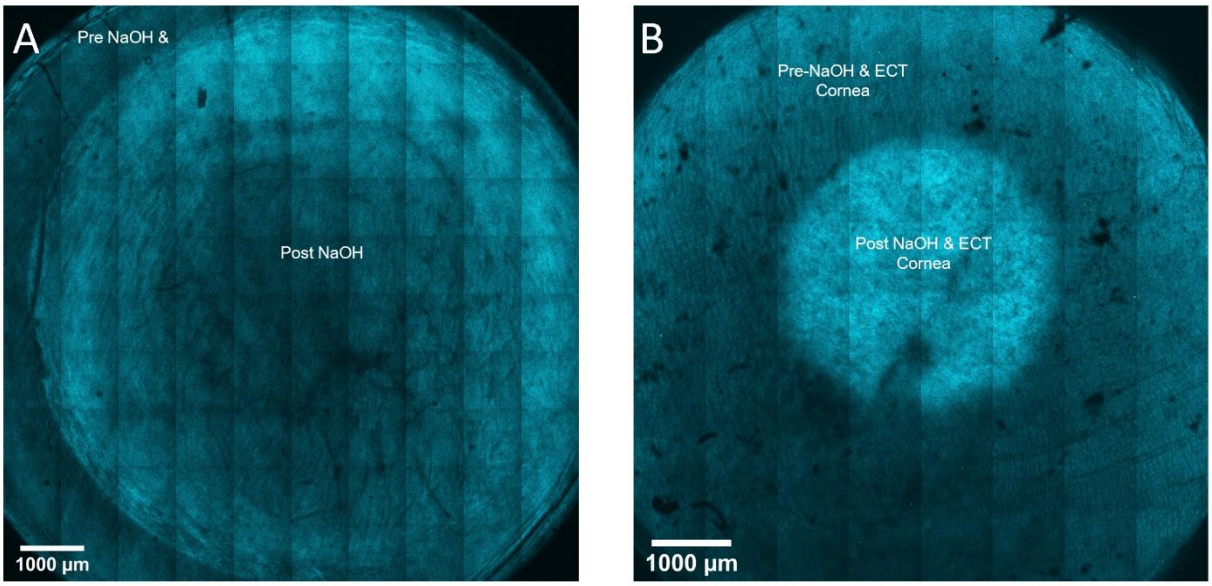

Figure 10: An overlap of cornea cross-sectional SHG images with before and after of alkaline treatment (**A**) and ECT treatment (**B**). ROIs were selected at the center of each tile for coherency coefficient analysis.

3.1.3 Discussion

The numerical analysis in the collagen fiber orientation in the negative control and cleared corneas, and native corneal tissue, suggests the mechanism for ECT mediated corneal clearing does not depend upon the collagen fibril alignment and orientation. Therefore, the macroscopic corneal structure is not affected by the corneal clearing via ECT electrodes. This can be seen in all sample protocols in Figures 8 and 9 after collagen analysis. If major structural change occurred within the stroma, the histogram's shape should have changed, presumably due to some electro-mechanical or pH effect. We observed no major change in the distribution as the date showed no significant preferred orientation. Collagen fibril orientation is observed to change to a bimodal distribution in pathologic cornea [32]. The

preservation of a unimodal, Gaussian distribution within the 150-micron slice throughout treatment reveals that the collagen fibril orientation is stable.

Collagen preferred orientation analysis with respect to corneal depth further supports this as for both negative control and ECT-treated tissue. NaOH-treated tissue had fibrils with preferred orientation ranging from -1.5 degrees to +2.5 degrees across the thickness of the cornea while the native sample had a range of -4.0 degree to +2.0 degrees. The most critical region of interest were depths from the surface to 200-microns as this includes stromal tissue. Little to no change in the collagen directionality was demonstrated as there were minimal differences in the preferred orientation ranges with -1.5 degrees to +2.0 degrees for the control and -1.5 degree to +2.5 degrees for the NaOH-treatment. Overall, the preferred orientations decreased with the alkaline exposure, but no significant directionality was determined. For the cleared sample and its control sample, the collagen preferred orientation ranged from -2.0 degrees to +1.5 degrees and -0.5 degrees to +3.5 degrees across the corneal depth respectively. Although the collagen directionality decreased overall throughout the various depths of the cornea for the NaOH+ECT treated samples, a major shift in fibril orientation was not seen.

Additional image analysis examined the corneal standard deviation in relation to corneal depth was like the preferred collagen orientation as there was minimal change throughout the tissue. For native cornea versus NaOH-treated cornea, the standard deviation of collagen orientation of the first fell between 31.5 degrees to 35 degrees while the latter had calculated values between 31 degrees to 35 degrees. Despite the slight decrease in the fibril orientations, the large standard deviation is retained throughout all layers of the

imaged tissue. This suggests that the collagen directionality is more spread out over a greater range of angles. The ECT-cleared and its control sample analysis resulted in an identical standard deviation ranges of 31.5 degrees to 34.5 degrees throughout the entire z-stack. There is an overall increase in standard deviation values in the NaOH+ECT treated tissue, but similar to the negative control, the large values still point to a wider spread for collagen angles. A high value for the standard deviation as observed in treatment groups suggests that the corneal collagens are not highly oriented under any of these conditions.

Coherency coefficients measured throughout the corneal thickness further supports the idea of collagen being less oriented for all samples. Negative control tissue had a determined coherency coefficient range from 0.03 to 0.05 while the native cornea had a range of 0.03 to 0.048. Minimal differences between the coherency coefficient suggests that collagen is not significantly altered by alkaline treatment. The ECT-treated cornea showed a greater decrease in coherency coefficients in comparison to the native tissue as analysis determined the former's range of 0.034 to 0.046 and the latter's range of 0.025 to 0.055. Even considering the largest difference between the coherency coefficients was 0.013 for the experimental group and 0.007 for the negative group, all determined values are closer to zero. For the coherency coefficient, if a value is close to one, then the analyzed tissue is highly organized. In this case, all fibrils from the control, negative-control, and experimental samples maintain a low-level of organization throughout the corneal depth and thus implies minimal rearrangement of the collagen fiber directionality.

3.2 Corneal Reshaping

3.2.1 Experimental Setup

White New Zealand rabbit eyes were also used for corneal reshaping experiments. Globes were extracted within three hours post-mortem and placed in 5% Hanks' Balanced Salt Solution (HBSS) at room temperature. Similar to corneal clearing studies, experiments and imaging were conducted within two hours for tissue results most similar to in-vivo.
The corneal surface was evaluated for superficial tissue injury by inspection that may have occurred prior to any treatments through SHG imaging. A specimen is rejected if major defects such as excessive scratches across the entire corneal surface or folds, which can result from trauma during extraction or from improper handling during imaging. Enucleated eyes were positioned with the cornea facing downward toward the objective lens in direct contact with the transparent cell culture dish. To maintain its position, retain moisture, and to prevent any creases on the cornea stemming from the weight of the globe, the eye was cushioned by a ring of saline-soaked sponge.

Globes were then placed on the platform of the Zeiss LSM 510 Meta inverted confocal microscope. The two-photon microscopy used an excitation wavelength of 920nm to observe the collagen fibrils. An initial cross-sectional 9000umm-by-9000um tile image at 150-micron depth was taken to establish the baseline condition of the corneal tissue. Afterwards, a 900um-by-900um z-stacks with a minimum thickness of 200 um and a 1um step between slices, were taken at the center of the previous tile image. Once all baseline images were captured, the globes were placed back into the saline solution to be prepared for electromechanical reshaping (EMR) treatment.

Globes were transferred with the cornea facing upwards to a customized 3D-printed jig with a concave cavity to keep the sample stable. Three prongs on the side of the jig served as guiding rails for the electrode contact used for reshaping. The assembly was then placed in a 100-mm wide crystallizing dish and filled with saline solution until the eye was completely submerged. Digital photography was not performed during this experiment since shape changes are not visible to the naked eye.

A customized contact lens electrode system where platinum was electroplated onto a nickel surface was used for corneal reshaping on the experimental group. A three-electrode system was utilized where the working platinum electrode, or the anode, and aluminum reference electrode were embedded within the contact to perform EMR. The auxiliary electrode, or the cathode, was outside of the contact, but submerged within the saline solution which provided electrical continuity. The anode was placed at the center of the contact divot where the corneal reshaping would occur which can be seen in Figure 11. An power supply was connected to the electrodes to control the current and voltage introduced to the globe and create the localized pH gradient from the anode.

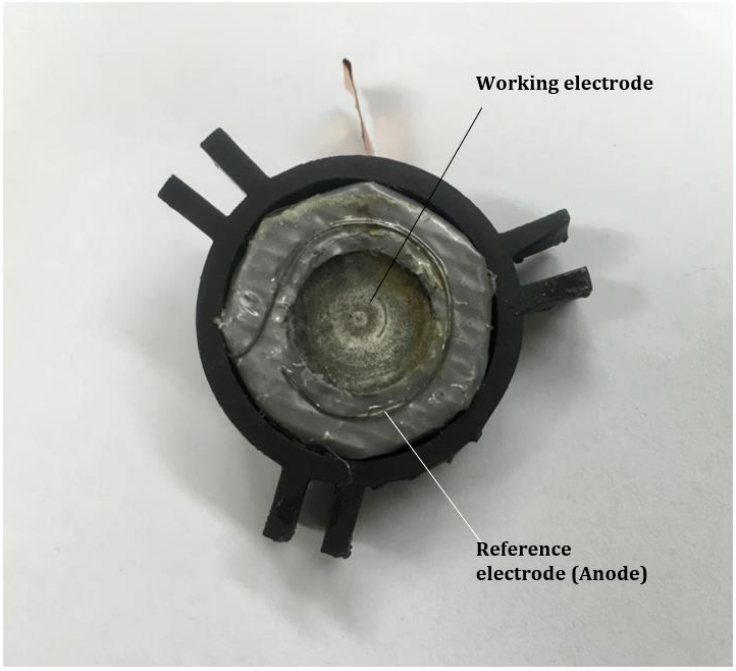

Figure 11: Contact that was used for EMR treatment of the cornea where the anode, or working electrode, is fixed at the center of the cornea and the reference is in contact with the surrounding saline. Electrodes were connected to the power supply via leads located at the top of the contact.

To reduce the risk of a constant voltage damaging the collagen fibrils, the current was pulsed into the sample. The current was supplied to the device for 5 seconds and then terminated for 30 seconds, allowing the redistribution of the newly generated acid. A voltage potential of 1.25V was used with a current of 0.2mA. The sample was pulsed until an accumulated charge of 0.2 C was recorded. SHG was repeated after each voltage application completed treatment to identify any changes in the structure of collagen. Collagen alignment data analysis was performed on the SHG images using ImageJ's plug-in, OrientationJ, and a customized MATLAB script.

3.2.2 Results

Initial qualitative analysis of the native corneal tissue SHG images showed strong blue signal throughout the cross-sectional tiled image, indicating a homogeneous collagen surface. Minor dark lines indicate regions of damage which were likely pre-existing and occurred during routine care in the vivarium; this did not interfere with the analysis of the corneal slices. EMR appeared to reduce the collagen signal in the center of the cornea where the working electrode was placed. Various areas of the cornea show the absence of a collagen signal, indicating that the collagen was altered from its optimal imaging positioning. Outside of the anode's ROI, the fibrils still give strong signal despite the new darkened areas. Figure 12 shows the before and after SHG tiles captured.

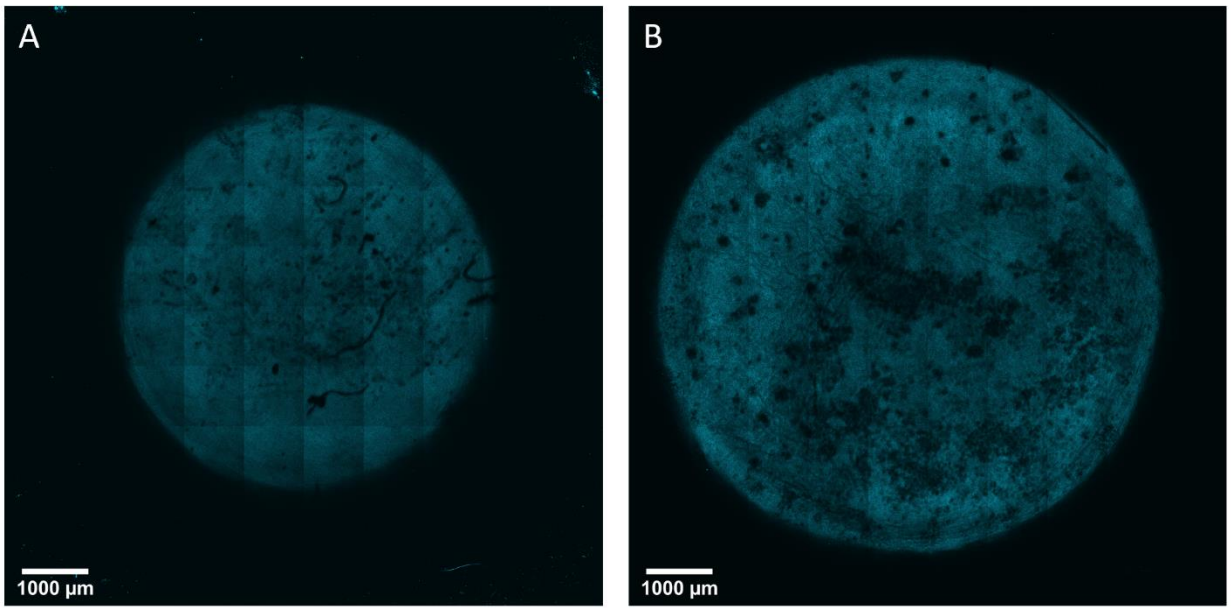

Figure 12: Control cross-sectional SHG image of the cornea (**A**) and reshaped tile image (**B**).

To measure the orientation of the collagen fibrils in the native and treated tissue, z-stacks taken at the center of the tile images. Histograms of both corneal conditions show that collagen fibers maintain a Gaussian distribution for orientation angle after treatment at a depth of 150 microns. Compared to native cornea tissue orientation, the EMR-treated tissue produced little change in collagen fibril direction, as the dominant collagen angle mean changed only by 1.38 degrees. The standard deviation of directionality had a small increase of 0.32 degrees. Table 2 shows the results of the degree analysis at a depth of 150-microns. These results suggest that the cornea's collagen organization and alignment are not affected by the in-situ oxidation-reduction reaction that was applied to create shape change. Analysis of the preferred orientation and its standard deviation with respect to tissue depth show minimal differences between experimental treatments and control (Figure 13, Figure 15).

Treatment	Collagen Orientation Mean (Degrees)	Collagen Orientation Standard Deviation (Degrees)	Coherency
Control	-0.0079	32.0734	0.048
ECT Reshape	1.3763	32.389	0.034

Table 2: Comparison of calculated values from SHG images taken at 150um depth of the native and EMR-treated cornea analyzed through ImageJ for collagen fibril orientation mean, standard deviation, and coherency..

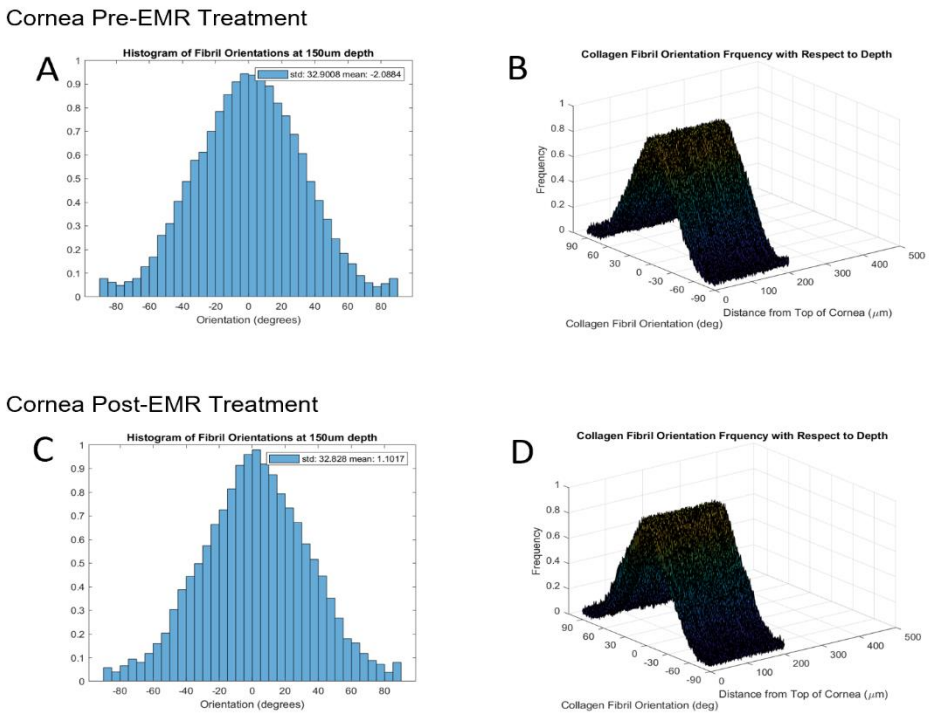

Figure 13: Post-image analysis on the SHG images displaying the collagen preferred orientation frequency histogram at 150-micron depth the orientation distribution changing with respect to depth. Row 1 gives data for the native cornea (A and B) while row 2 shows data for the EMR-treated cornea (C and D) respectively.

A comparison between specific ROIs pre and post EMR was performed to determine if significant changes in collagen structure were observed throughout the depth of the corneal stroma. EMR cornea tile was overlapped with the native corneal SHG image. A 900um-by-900um square-ROI was generated at each image center. Once these images were transposed over one another, the overlapping area of the centered squares was selected as the ROI for z-stack analysis (Figure 14). This ensured consistency in the areas chosen for processing. OrientationJ was used to determine the ROI's coherency coefficient (Table 2) for the different treatments. The coherency coefficient indicates if collagen fibers in the ROI have a preferred orientation if the coefficient is close to 1 [31]. The reshaped cornea had decreased coherency coefficient (-0.14) compared to the native cornea. Inasmuch as both

coherency coefficients were closer to 0 rather than 1, there is thus no significant change in preferred orientation of the collagen fibers.

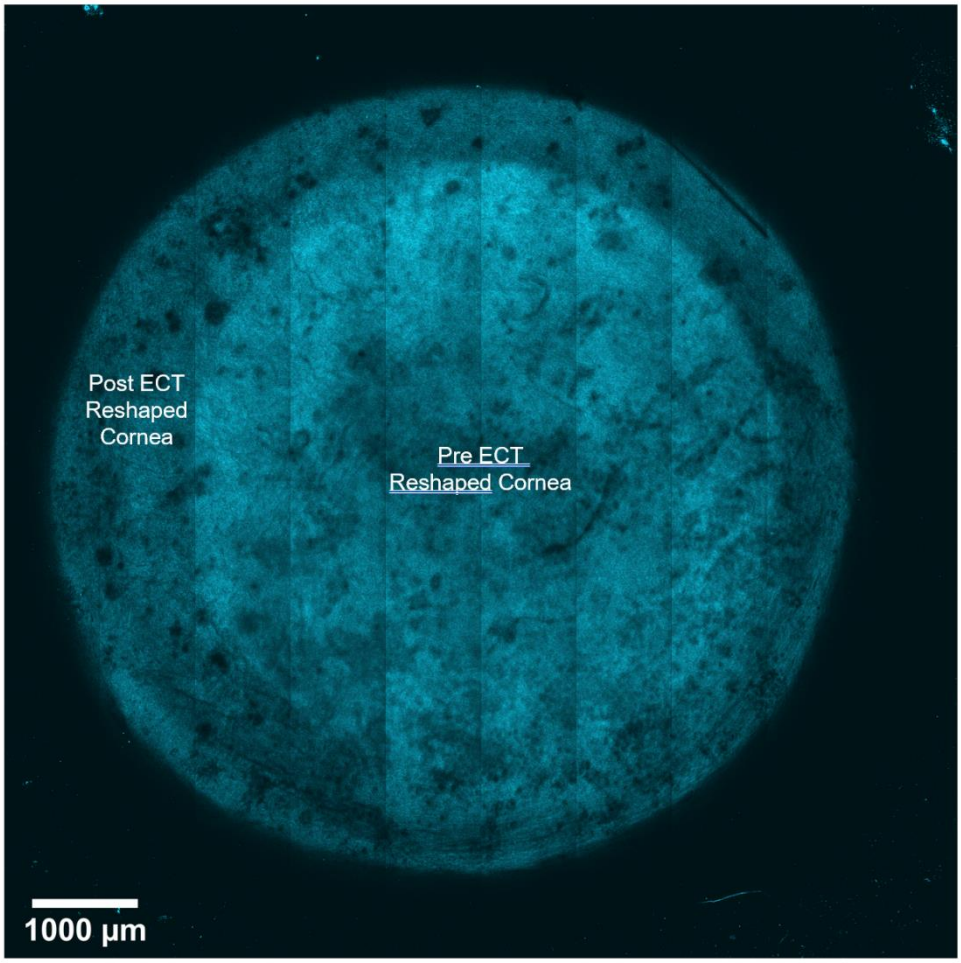

***Figure 14**:* Native and treated corneal cross-sectional SHG tiles transposed on top of each other to determine the ROI for coherency coefficient calculations

3.2.3 Discussion

Qualitatively, EMR groups had a weaker SHG signal. This indicates a certain level of rearrangement has occurred within the collagen fibrils to disrupt the optimal molecular structure that produces strong signal. With corneal reshaping, it is critical to understand how stromal collagen orientation changes from the SHG data. The orientation analysis showed a

shift of the preferred orientation changes from -.008 degrees to +1.38 degrees at 150-micron depth within the cornea's stroma and minimal decrease in the standard deviation by 0.32 degrees. These shifts in the collagen orientation mean and collagen orientation standard deviation suggests that the collagen structure is primarily preserved during the EMR process. In Figure 15, difference in collagen orientation as a function of stromal depth between native and EMR tissue do not appear to be significant. Inspection of collagen fibril orientation histograms show the preservation of a unimodal, Gaussian distribution between the native and treated cornea and suggests no structural change is occurring within the stroma. Native corneal tissues have a dominant preferred orientation of their collagen fibrils whereas diseased corneas may have random collagen orientation [32]. By not disrupting the orientation of the collagen fibers, the effect of EMR on corneal functionality is limited to superficial corneal change to correct the refractive error.

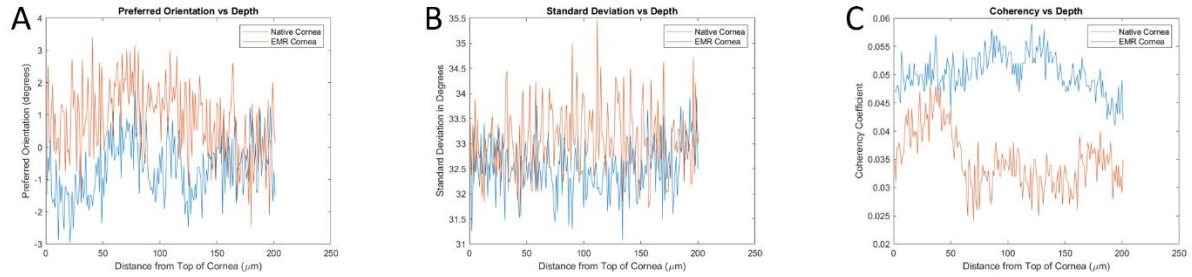

***Figure 15**:* Representations of collagen fibril orientations showing collagen preferred orientation (A), standard deviation (B), and coherency coefficient (C) with respect to depth of both native (shown in blue) and treated tissue (shown in orange).

Analysis on the corneal collagen fiber standard deviation values with respect to depth showed a similar trend: the preferred collagen orientation did not significantly change with depth. However, all calculated standard deviations values were between 31 and 34 degrees, which indicates that although there is a prominent preferred orientation in all corneal layers, the orientation angles are spread out over a wider numerical range. The data collected from

this coherency analysis provides further evidence that there is a weaker preferred orientation throughout the corneal slices for native and EMR-treated tissue. Coherency coefficients measured throughout the entire 200-micron z-stack depth showed minute differences between native tissue (0.04 to 0.06) and treated cornea (0.02 to 0.05). Even considering the largest difference calculated between the coherency coefficients of 0.033, the values are all close to 0, indicating that the collagen is not highly oriented for both treatments.

Chapter 4: Conclusion and Future Work

4.1 Summary and Conclusion

Structure, shape intefrity, refraction and optical clarity are all interlinked and depend upon corneal collagen structure at many spatial scales. Understanding these interactions is needed to develop novel treatments for diseases of the eye. Second Harmonic Generation (SHG) imaging as it is non-invasive, can penetrate deep into the tissue, requires no additional dyes, and has little to no phototoxicity effects on tissue samples. It is an ideal technology to evaluate corneal collagens. Because of this, fresh ex-vivo tissue samples may be imaged, and tissue can be examined in largely its native state, whereas traditional light microscopy requires sample fixation. This thesis explored the use of SHG imaging to examine how the collagens of the cornea change during electrochemically-mediated clearing and reshaping technologies.

For the corneal clearing experiment, ex-vivo rabbit eyes were exposed to NaOH as the negative control while treatment of NaOH with electrochemical therapy (ECT) was the experimental group. For every specimen SHG images were acquired before and after intervention. SHG image analysis on the collage orientation showed the alkaline exposure caused an increase in the collage fiber orientation mean and standard deviation within about 2 degrees. On the other hand, the NaOH+ECT treated sample had an overall decrease in collagen preferred orientation within 4 degrees and an increased standard deviation within 1 degree. Although there are shifts in fibril directionality, all corneas maintained a unimodal distribution throughout a 200-micron cross section of the stroma. This suggests that despite the slight shifts in preferred orientations and standard deviations, the corneas did not

experience significant change to their structures as rearranged collagen fibrils would either dramatically shift their directionality or have a different distributions with respect to depth. Calculated coherency coefficients also stated that all tissues kept values close to zero throughout the corneal thickness, further supporting that no structural change was made to make the fibrils be strongly organized.

For the corneal reshaping experiment, extracted rabbit globes had the corneal surface reshaped through EMR by using a platinum plated contact. A baseline control SHG images were captured prior to any treatment then compared against post-treatment images. Analysis of collagen directionality from SHG revealed that the preferred orientation of the fibrils as well as their standard deviation experienced a minimal increase within 1.5 degrees. This shift is insignificant as the fibril orientation retains a unimodal distribution throughout all layers of the cornea, suggesting that EMR modestly at best rearranged the collagen and changed the tissue's structure. The calculated coherency coefficient had a similar result where both the pre- and post-treatment tissue-maintained values close to zero throughout the entire cornea, demonstrating that no significant geometric rearrangements were seen to make the collagen fibrils more highly organized.

Major limitations observed during this study are the lack of standardization in experimental design for both corneal clearing and reshaping. Optimization of experimental design and treatment dosimetry will be required to ensure consistent clearing results and cornea positioning for imaging. Reliance on SHG for data analysis may not provide the appropriate quantitative information regarding the integrity of the tissue ROI as it only general macroscopic data. Additionally, SHG z-stack imaging potentially provides inaccurate

comparison between control and treated samples as the step depth used may be too large and miss the affected area if significant swelling of the collagen fibrils occurs.

4.2 Future Work

Findings from this study are a stepping-stone to demonstrate the viability of these novel-treatments for optical errors. Future experiments will need to focus on comparing the viability of the tissue and cells before and after the introduction of a pH gradient. This will be critical in corneal clearing as it determines if the alkaline-damaged tissue is further damaged from ECT treatment. As for corneal reshaping, it will need to be determined if shape change achieved with limited cellular injury or spatially localized tissue damage.

Another critical future work will be to study whether the changes made to the cornea in both corneal clearing and reshaping are sustainable. An in-vivo study would be the best experimental setup to analyze this as ex-vivo tissues will die over time if not cultured. SHG will allow insight to determine if the collagen itself changes over time to revert back to either it's native or damaged state depending on the experiment. If the applied change is sustainable in the tissue, the eye functionality can also be evaluated to determine if these novel treatments provide an alternative permanent solution.

References

[1] J. I. Clark, "Order and disorder in the transparent media of the eye," *Experimental Eye Research*, vol. 78, no. 3. Academic Press, pp. 427–432, 01-Mar-2004.

[2] G. O. . Naumann and D. J. Apple, *Pathology of the Eye*. Springer-Verlag New York, Inc, 1986.

[3] M. Ahearne and A. P. Lynch, "Early Observation of Extracellular Matrix-Derived Hydrogels for Corneal Stroma Regeneration," *Tissue Eng. - Part C Methods*, vol. 21, no. 10, pp. 1059–1069, 2015.

[4] K. M. Meek and C. Knupp, "Corneal structure and transparency," *Progress in Retinal and Eye Research*, vol. 49. Elsevier Ltd, pp. 1–16, 2015.

[5] Y. Qazi, G. Wong, B. Monson, J. Stringham, and B. K. Ambati, "Corneal transparency: Genesis, maintenance and dysfunction," *Brain Research Bulletin*, vol. 81, no. 2–3. NIH Public Access, pp. 198–210, 15-Feb-2010.

[6] T. H. Dohlman, J. Yin, and R. Dana, "Methods for Assessing Corneal Opacity," *Seminars in Ophthalmology*, vol. 34, no. 4. Taylor and Francis Ltd, pp. 205–210, 19-May-2019.

[7] G. Clare, H. Suleman, C. Bunce, and H. Dua, "Amniotic membrane transplantation for acute ocular burns," *Cochrane Database of Systematic Reviews*, vol. 2012, no. 9. John Wiley and Sons Ltd, 12-Sep-2012.

[8] P. Singh, M. Tyagi, Y. Kumar, K. Gupta, and P. Sharma, "Ocular chemical injuries and their management," *Oman Journal of Ophthalmology*, vol. 6, no. 2. Wolters Kluwer -- Medknow Publications, pp. 83–86, 2013.

[9] A. Baradaran-Rafii, M. Eslani, Z. Haq, E. Shirzadeh, M. J. Huvard, and A. R. Djalilian, "Current and Upcoming Therapies for Ocular Surface Chemical Injuries," *Ocular Surface*, vol. 15, no. 1. Elsevier Inc., pp. 48–64, 01-Jan-2017.

[10] Y. Mashima, M. Kawai, and M. Yamada, "Corneal electrolysis for recurrence of corneal stromal dystrophy after keratoplasty," *Br. J. Ophthalmol.*, vol. 86, no. 3, pp. 273–275, 2002.

[11] Y. Mashima, M. Kawashima, and M. Yamada, "Electrolytic removal of recurrence of granular corneal dystrophy," *Eye*, vol. 17, no. 8, pp. 975–981, 2003.

[12] "Eye Health Statistics - American Academy of Ophthalmology." [Online]. Available: https://www.aao.org/newsroom/eye-health-statistics. [Accessed: 05-Aug-2020].

[13] J. Cooper and A. V. Tkatchenko, "A Review of Current Concepts of the Etiology and Treatment of Myopia," *Eye Contact Lens*, vol. 44, no. 4, pp. 231–247, Jul. 2018.

[14] "Astigmatism | AOA." [Online]. Available: https://www.aoa.org/healthy-eyes/eye-and-vision-conditions/astigmatism?sso=y. [Accessed: 15-Aug-2020].

[15] J. M. Wilkinson, E. W. Cozine, and A. R. Khan, "Refractive Eye Surgery: Helping Patients Make Informed Decisions About LASIK," May 2017.

[16] J. S. Wolffsohn and L. N. Davies, “Presbyopia: Effectiveness of correction strategies,” *Progress in Retinal and Eye Research*, vol. 68. Elsevier Ltd, pp. 124–143, 01-Jan-2019.

[17] “LASIK eye surgery - Mayo Clinic.” [Online]. Available: https://www.mayoclinic.org/tests-procedures/lasik-eye-surgery/about/pac-20384774. [Accessed: 18-Aug-2020].

[18] A. M. Karamzadeh, J. C. Chang, S. Diaz, T. E. Milner, and B. J. F. Wong, “Long-term in vivo stability of rabbit nasal septal cartilage following laser cartilage reshaping: A pilot investigation,” *Lasers Surg. Med.*, vol. 36, no. 2, pp. 147–154, Feb. 2005.

[19] T. D. Nguyen, A. C. Hu, D. E. Protsenko, and B. J. F. Wong, “Effects of electromechanical reshaping on mechanical behavior of exvivo bovine tendon,” *Clin. Biomech.*, vol. 73, pp. 92–100, Mar. 2020.

[20] D. Hutchison et al., "Electrochemolipolysis of Human Adipose Tissue", *Facial Plastic Surgery & Aesthetic Medicine*, vol. 22, no. 2, pp. 86-92, 2020.

[21] T. T. Pham *et al.*, “The biophysical effects of localized electrochemical therapy on porcine skin,” *J. Dermatol. Sci.*, vol. 97, no. 3, pp. 179–186, Mar. 2020.

[22] D. Protsenko, K. Ho and B. Wong, "Stress Relaxation in Porcine Septal Cartilage During Electromechanical Reshaping: Mechanical and Electrical Responses", *Annals of Biomedical Engineering*, vol. 34, no. 3, pp. 455-464, 2006.

[23] R. Li, X. Wang, Y. Zhou, H. Zong, M. Chen, and M. Sun, “Advances in nonlinear optical microscopy for biophotonics,” *J. Nanophotonics*, vol. 12, no. 03, p. 1, Aug. 2018.

[24] X. Chen, O. Nadiarynkh, S. Plotnikov, and P. J. Campagnola, “Second harmonic generation microscopy for quantitative analysis of collagen fibrillar structure,” *Nat. Protoc.*, vol. 7, no. 4, pp. 654–669, Apr. 2012.

[25] P. Campagnola, “Second harmonic generation imaging microscopy: Applications to diseases diagnostics,” *Anal. Chem.*, vol. 83, no. 9, pp. 3224–3231, May 2011.

[26] S. Ranjit *et al.*, “Imaging Fibrosis and Separating Collagens using Second Harmonic Generation and Phasor Approach to Fluorescence Lifetime Imaging,” *Sci. Rep.*, vol. 5, Aug. 2015.

[27] C. Y. Park, J. K. Lee, and R. S. Chuck, “Second harmonic generation imaging analysis of collagen arrangement in human cornea,” *Investig. Ophthalmol. Vis. Sci.*, vol. 56, no. 9, pp. 5622–5629, 2015.

[28] R. Rezakhaniha *et al.*, “Experimental investigation of collagen waviness and orientation in the arterial adventitia using confocal laser scanning microscopy,” *Biomech. Model. Mechanobiol.*, vol. 11, no. 3–4, pp. 461–473, Mar. 2012.

[29] D. Lubeck and J. S. Greene, “Corneal injuries,” *Semin. Ophthalmol.*, vol. 5, no. 2, pp. 61–73, Feb. 1990.

[30] "Chemical Injuries of the Cornea: Classification Schemes." [Online]. Available: https://www.aao.org/focalpointssnippetdetail.aspx?id=7dabd8e2-6282-4d1d-9a97-c43b43f909f8. [Accessed: 29-Aug-2020].

[31] E. Fonck *et al.*, "Effect of aging on elastin functionality in human cerebral arteries," *Stroke*, vol. 40, no. 7, pp. 2552–2556, Jul. 2009.

[32] F. J. Ávila, P. Artal, and J. M. Bueno, "Quantitative discrimination of healthy and diseased corneas with second harmonic generation microscopy," *Tra*